# $qq\bar{q} \to qq\bar{q}$ and $q\bar{q}\bar{q} \to q\bar{q}\bar{q}$ Elastic Scatterings and Thermalization of Quark Matter and Antiquark Matter

Xiao-Ming Xu[a], Cheng-Cheng Ma[a], An-Qian Chen[b], H.J. Weber[c]

[a]Department of Physics, Shanghai University, Baoshan, Shanghai 200444, China
[b]Department of Communication, Shanghai University, Baoshan, Shanghai 200444, China
[c]Department of Physics, University of Virginia, Charlottesville, VA 22904, U.S.A.



**Abstract**

Thermalization of quark matter and antiquark matter is studied with quark-quark-antiquark as well as quark-antiquark-antiquark elastic scatterings. Squared amplitudes of $qq\bar{q} \to qq\bar{q}$ and $q\bar{q}\bar{q} \to q\bar{q}\bar{q}$ at order $\alpha_s^4$ are derived in perturbative QCD. Solved by a new technique, solutions of transport equations with the squared amplitudes indicate that the scatterings $qq\bar{q} \to qq\bar{q}$ and $q\bar{q}\bar{q} \to q\bar{q}\bar{q}$ shorten the thermalization time of quark matter and antiquark matter. It is emphasized that three-parton and other multi-parton scatterings become important at the high parton number density achieved in RHIC Au-Au collisions.

PACS codes: 24.85.+p; 12.38.Mh; 25.75.Nq
Keywords: quark and antiquark matter; quark-quark-antiquark elastic scattering; transport equation; thermalization

## 1. Introduction

Establishing a thermal state is critical in the formation of a quark-gluon plasma [1,2]. Initial high-energy heavy-ion collisions create deconfined matter which is not in thermal and chemical equilibrium. The problem of quark-gluon matter thermalization was studied early in parton dynamics in Refs. [3,4]. The 2-to-2 and 2-to-3 gluon scatterings produce a gluon-matter thermalization time greater than 1 fm/c [5-7]. In accounting for the elliptic flow of hadrons observed in Au-Au collisions at the Relativistic Heavy Ion Collider (RHIC), recent hydrodynamic calculations come to the conclusion that the thermalization of quark-gluon matter is finished within the time of 1 fm/c [8-11]. The thermalization process is fascinating and needs to be understood urgently. We have proposed 3-to-3 as well as 2-to-2 quark elastic scatterings to study the thermalization of quark matter [12]. But a thermalization time of about 1.8 fm/$c$ is obtained from the mechanism. How rapid thermalization of quark matter comes about from quark scatterings is still a difficult and complicated task to explain. In this letter we include quark-quark-antiquark and quark-antiquark-antiquark elastic scatterings in an effort to understand better the thermalization of both quark and antiquark matter independent of gluon matter.

We present four new aspects. The first is to recognize the importance of multi-parton scatterings at a high parton number density; the second is to calculate perturbatively the squared amplitudes of quark-quark-antiquark elastic scatterings which subsequently give the squared amplitudes of quark-antiquark-antiquark elastic scatterings; the third is to solve transport equations with a new technique; the fourth is to provide a new form for the formula of the interaction range of three-parton scattering. The squared amplitudes are derived by Fortran codes that implement the QCD Feynman rules. The new technique deals with a multi-parton scattering in terms of a sphere that moves with a particle. These four aspects form an integral part of our study of the thermalization of quark and antiquark matter.

## 2. Probability of multi-parton scatterings

The rapid thermalization is related to high gluon number density [13-15] at which triple-gluon elastic scatterings lead to a short thermalization time [16]. The importance of three-gluon scatterings is implied and we can thus speculate on possible or even sizeable contributions of other multi-gluon scatterings. We therefore give a Monte Carlo test on the occurrence of multi-parton scatterings from a parton distribution that is anisotropic in momentum space and inhomogeneous in coordinate space, as created in initial collisions of two Lorentz-contracted gold nuclei. Such a parton distribution has been generated by HIJING [17] for central Au-Au collisions at $\sqrt{s_{NN}} = 200$ GeV and cast into the form [18]

$$f(k_\perp, y, r, z, t) = \frac{1}{16\pi R_A^2} g(k_\perp, y) \frac{e^{-(z - t\tanh y)^2/2\Delta_k^2}}{\sqrt{2\pi}\Delta_k}, \tag{1}$$

with

$$\Delta_k \approx \frac{2}{k_\perp \cosh y}$$

and

$$g(k_\perp, y) = \frac{(2\pi)^3}{k_\perp \cosh y} \frac{dN}{dy d^2k_\perp},$$

where the gold nucleus radius is $R_A$=6.4 fm, and $k_\perp$, $y$, $t$, $z$ and $r$ are transverse momentum, rapidity, time, coordinate and radius in the transverse direction, respectively. One thousand and five hundred gluons are created from the distribution $f(k_\perp, y, r, z, 0.2\ \mathrm{fm}/c)$ by the rejection method within $-0.3\ \mathrm{fm} < z < 0.3\ \mathrm{fm}$ in the longitudinal direction and $r < R_A$ in the transverse direction. This volume of partons corresponds to a parton number density of 19.4 $\mathrm{fm}^{-3}$. At such high density, we have to examine the occurrence of multi-parton scatterings. We assume a scattering of two partons when the distance of the two partons is less than a given interaction range. If $n$ partons are within a sphere of which the center is at the center of mass of the $n$ partons and of which the radius equals the given interaction range, a scattering of the $n$ partons is taken to occur. When the scattering of $n$ partons with a certain value of $n$ is counted, other multi-parton scatterings are excluded. Therefore, the maxima of the numbers of 2-parton, 3-parton, 4-parton, 5-parton, 6-parton and 7-parton scatterings at a given time are 750, 500, 375, 300, 250 and 214, respectively, which give a sum of 2389. The numbers of $n$-parton scatterings with $n = 2, \cdots, 7$ at $t = 0.2\ \mathrm{fm}/c$ are denoted each by $m_n$ and plotted in Fig. 1. When the interaction range increases, more scatterings of not only two but also seven partons happen. All the scattering numbers saturate at an interaction range of 0.6 fm except for the three-parton scattering number which saturates at a smaller interaction range. If we consider the practical case when 2-parton scattering, 3-parton scattering, etc. may happen at the same time, we need to estimate the probability of $n$-parton scattering. A guide for this probability is provided by $R_n = m_n/2389$, the ratio of the $n$-parton scattering number obtained above to the total number 2389. This ratio is drawn in Fig. 2. For an interaction range larger than 0.15 fm, the three-parton scattering becomes important in comparison to the two-parton scattering. At an interaction range of 0.62 fm, which acts as the radius of a unit volume of sphere, the 2-parton scattering has the occurrence probability of 30 %, the 3-parton scattering 20 %, the 4-parton scattering 14.6 %, and even the 7-parton scattering has 7.5 %. The scattering numbers and the ratios shown in Figs. 1 and 2 lead to the high parton number density of 19.4 $\mathrm{fm}^{-3}$ which implies a substantial occurrence of multi-parton scatterings.

## 3. Quark-quark-antiquark elastic scatterings

In Figs. 3 and 4 ten diagrams are plotted to show the elastic scattering of quark-quark-antiquark at order $\alpha_s^4$. The eight diagrams in Fig. 3 are related to two successive gluon exchanges and the two diagrams in Fig. 4 involve a triple gluon coupling. If the two initial or final quarks have the same flavor, the exchange of the two quarks generates other diagrams which are not displayed in Figs. 3 and 4. For $\mathrm{uu\bar{u}} \to \mathrm{uu\bar{u}}$, we must take into account 38 diagrams of which 28 diagrams contain quark-antiquark annihilation and creation, and then confront a cumbersome derivation of the squared amplitude for the scattering $q(p_1) + q(p_2) + \bar{q}(-p_3) \to q(p_4) + q(p_5) + \bar{q}(-p_6)$, where $p_\mathrm{i} = (E_\mathrm{i}, \vec{p}_\mathrm{i})$ is the quark four-momentum.

As an example, the derivation of the squared amplitude of the last diagram in Fig. 3 is described here. Denote by $q_1$, $g$ and $\lambda$ the momentum, color and space-time index of the gluon created by the annihilation of the initial quark and antiquark, by $q_3$, $h$ and $\sigma$ of the other gluon, and by $q_2$ the momentum of the quark propagator, respectively. With the Feynman rules given in Ref. [19], the first Fortran code is designed to construct the

spin- and color-summed squared amplitude

$$\sum_{\rm spins,colors} \mid \mathcal{M}_{\rm F_{*-}} \mid^2 = \frac{{\rm g_s^8}}{q_1^4 q_2^4 q_3^4} \sum_{\rm colors} tr(T_g T_h T_{h'} T_{g'}) tr(T_h T_{h'}) tr(T_g T_{g'})$$
$$tr(\gamma_\lambda \not{q}_2 \gamma_\sigma \not{p}_1 \gamma_{\sigma'} \not{q}_2 \gamma_{\lambda'} \not{p}_4) tr(\gamma_\sigma \not{p}_6 \gamma_{\sigma'} \not{p}_5) tr(\gamma_\lambda \not{p}_2 \gamma_{\lambda'} \not{p}_3), \qquad (2)$$

where $T_g$ etc. are the color SU(3) group generators, $\rm g_s$ is the quark-gluon coupling constant and $\rm g_s^2 = 4\pi\alpha_s$, respectively. The Dirac gamma matrices $\gamma_\lambda$ and $\gamma_\sigma$ in $\mathcal{M}_{\rm F_{*-}}$ are indicated by $\gamma_{\lambda'}$ and $\gamma_{\sigma'}$ in $\mathcal{M}^+_{\rm F_{*-}}$. The calculation of the traces is lengthy and cumbersome, but the second Fortran code is designed to accomplish the task. The Fortran code produces

$$\sum_{\rm colors} tr(T_g T_h T_{h'} T_{g'}) tr(T_h T_{h'}) tr(T_g T_{g'}) = \frac{4}{3},$$

which agrees with the result derived by hand. Including the average over the spin and color states of the two initial quarks and the initial antiquark, the spin- and color-summed squared amplitude is

$$\frac{1}{8}\frac{1}{27} \sum_{\rm spins,colors} \mid \mathcal{M}_{\rm F_{*-}} \mid^2 = \frac{16{\rm g_s^8}}{81}(-u_{16}u_{26}u_{34}^2 + u_{16}u_{24}u_{34}u_{35} + u_{16}u_{24}u_{34}^2$$
$$-u_{16}u_{24}u_{26}u_{34} + u_{16}u_{24}^2 u_{35} + u_{16}u_{24}^2 u_{34}$$
$$-2u_{16}^2 u_{24}u_{34} + u_{15}u_{26}u_{34}^2 - u_{15}u_{24}u_{34}u_{35}$$
$$+u_{15}u_{24}u_{34}^2 + u_{15}u_{24}u_{26}u_{34} - u_{15}u_{24}^2 u_{35}$$
$$+u_{15}u_{24}^2 u_{34} - 2u_{15}^2 u_{24}u_{34} - s_{31}u_{15}u_{24}u_{34}$$
$$-s_{31}u_{15}u_{24}^2 - s_{23}u_{16}u_{26}u_{34} + s_{23}u_{16}u_{24}u_{35}$$
$$+2s_{23}u_{16}u_{24}u_{34} + s_{23}u_{16}u_{24}^2 - s_{23}u_{16}^2 u_{34}$$
$$-s_{23}u_{16}^2 u_{24} + s_{23}u_{15}u_{34}^2 + s_{23}u_{15}u_{26}u_{34}$$
$$-s_{23}u_{15}u_{24}u_{35} + 2s_{23}u_{15}u_{24}u_{34} - s_{23}u_{15}^2 u_{34}$$
$$-s_{23}u_{15}^2 u_{24} - s_{23}s_{31}u_{15}u_{24} + s_{23}^2 u_{16}u_{24}$$
$$+s_{23}^2 u_{15}u_{34} - s_{12}u_{16}u_{34}^2 - s_{12}u_{16}u_{24}u_{34} - s_{12}s_{23}u_{16}u_{34})$$
$$/[s_{23}(s_{23} + u_{21} + u_{31})(s_{23} - u_{12} - u_{13} + u_{21} + u_{31})]^2, \qquad (3)$$

which displays the shortest expression among all the individually squared amplitudes of the diagrams in Figs. 3 and 4, and the nine independent Lorentz-invariant momentum variables $s_{12} = (p_1+p_2)^2$, $s_{23} = (p_2+p_3)^2$, $s_{31} = (p_3+p_1)^2$, $u_{15} = (p_1-p_5)^2$, $u_{16} = (p_1-p_6)^2$, $u_{24} = (p_2-p_4)^2$, $u_{26} = (p_2-p_6)^2$, $u_{34} = (p_3-p_4)^2$ and $u_{35} = (p_3-p_5)^2$. Interference of amplitudes of different diagrams totals 1004 nonzero terms. These interference terms are derived with the Fortran codes. The spin- and color-averaged squared amplitude of every diagram and the interference terms of different diagrams are used in the transport equation to study the effects of quark-quark-antiquark elastic scatterings.

## 4. Transport equation

Quark matter is assumed to have equal up-quark and down-quark distributions. The same assumption applies to antiquark matter. The mutual dependence of the evolution of

quark matter and antiquark matter derives from the two-body and three-body scatterings of quarks and antiquarks. With the assumption that the quark distribution in quark matter is the same as the antiquark distribution in antiquark matter, the variation of the up-quark distribution $f_1$ is described by the transport equation

$$
\begin{aligned}
&\frac{\partial f_1}{\partial t} + \vec{\rm v}_1 \cdot \vec{\nabla}_{\vec{r}} f_1 \\
&= -\frac{\rm g_Q}{2E_1} \int \frac{d^3p_2}{(2\pi)^3 2E_2} \frac{d^3p_3}{(2\pi)^3 2E_3} \frac{d^3p_4}{(2\pi)^3 2E_4} (2\pi)^4 \delta^4(p_1+p_2-p_3-p_4) \\
&\quad \times (\frac{1}{2} \mid \mathcal{M}_{\rm uu\to uu} \mid^2 + \mid \mathcal{M}_{\rm ud\to ud} \mid^2 + \mid \mathcal{M}_{\rm u\bar{u}\to u\bar{u}} \mid^2 + \mid \mathcal{M}_{\rm u\bar{d}\to u\bar{d}} \mid^2) \\
&\quad \times [f_1 f_2 (1-f_3)(1-f_4) - f_3 f_4 (1-f_1)(1-f_2)] \\
&\quad - \frac{\rm g_Q^2}{2E_1} \int \frac{d^3p_2}{(2\pi)^3 2E_2} \frac{d^3p_3}{(2\pi)^3 2E_3} \frac{d^3p_4}{(2\pi)^3 2E_4} \frac{d^3p_5}{(2\pi)^3 2E_5} \frac{d^3p_6}{(2\pi)^3 2E_6} \\
&\quad \times (2\pi)^4 \delta^4(p_1+p_2+p_3-p_4-p_5-p_6) \\
&\quad \times [\frac{1}{12} \mid \mathcal{M}_{\rm uuu\to uuu} \mid^2 + \frac{1}{4} (\mid \mathcal{M}_{\rm uud\to uud} \mid^2 + \mid \mathcal{M}_{\rm udu\to udu} \mid^2) + \frac{1}{4} \mid \mathcal{M}_{\rm udd\to udd} \mid^2 \\
&\quad + \frac{1}{2} \mid \mathcal{M}_{\rm uu\bar{u}\to uu\bar{u}} \mid^2 + \frac{1}{2} \mid \mathcal{M}_{\rm uu\bar{d}\to uu\bar{d}} \mid^2 + \mid \mathcal{M}_{\rm ud\bar{u}\to ud\bar{u}} \mid^2 + \mid \mathcal{M}_{\rm ud\bar{d}\to ud\bar{d}} \mid^2 \\
&\quad + \frac{1}{4} \mid \mathcal{M}_{\rm u\bar{u}\bar{u}\to u\bar{u}\bar{u}} \mid^2 + \frac{1}{2} (\mid \mathcal{M}_{\rm u\bar{u}\bar{d}\to u\bar{u}\bar{d}} \mid^2 + \mid \mathcal{M}_{\rm u\bar{d}\bar{u}\to u\bar{d}\bar{u}} \mid^2) + \frac{1}{4} \mid \mathcal{M}_{\rm u\bar{d}\bar{d}\to u\bar{d}\bar{d}} \mid^2] \\
&\quad \times [f_1 f_2 f_3 (1-f_4)(1-f_5)(1-f_6) - f_4 f_5 f_6 (1-f_1)(1-f_2)(1-f_3)],
\end{aligned}
\tag{4}
$$

where the degeneracy factor ${\rm g_Q} = 6$ and the velocity of a massless up-quark $v_1 = 1$. The distribution function $f_{\rm i}$ is a function of the position $\vec{r}_{\rm i}$, the momentum $\vec{p}_{\rm i}$ and the time $t$. The 2-to-2 parton scatterings and the 3-to-3 scatterings are represented by the first and the second terms on the right-hand side of the above equation, respectively. Equations for down-quark, up-antiquark and down-antiquark are written in a similar way. The squared amplitudes for the 2-to-2 scatterings are the spin- and color-averaged squared amplitudes of order $\alpha_{\rm s}^2$ obtained in Refs. [20,21].

The squared amplitudes $\mid \mathcal{M}_{\rm uuu\to uuu} \mid^2$, $\mid \mathcal{M}_{\rm uud\to uud} \mid^2$, $\mid \mathcal{M}_{\rm udu\to udu} \mid^2$ and $\mid \mathcal{M}_{\rm udd\to udd} \mid^2$ were obtained in the study of triple-quark elastic scatterings [12]. The calculation of $\mid \mathcal{M}_{\rm uu\bar{u}\to uu\bar{u}} \mid^2$ requires the individually squared amplitude of every diagram in Figs. 3 and 4 and their interference terms, and the other diagrams arising from the exchange of the two quarks are also included. The squared amplitude $\mid \mathcal{M}_{\rm uu\bar{d}\to uu\bar{d}} \mid^2$ is based on diagrams $F_-$, $F_+$ and $F_*$ and the diagrams generated from the three diagrams via the exchange(s) of the two initial quarks and/or the two final quarks; $\mid \mathcal{M}_{\rm ud\bar{u}\to ud\bar{u}} \mid^2$ is based on $F_-$, $F_+$ and $F_*$ and the diagrams generated from all the diagrams in Figs. 3 and 4 via the exchange of the left quark line and the right quark line; $\mid \mathcal{M}_{\rm ud\bar{d}\to ud\bar{d}} \mid^2$ is based on all the diagrams in Figs. 3 and 4 and the two diagrams generated from $F_-$ and $F_+$ via the exchange of both the left quark line and the right quark line. Since the calculation of $\mid \mathcal{M}_{\rm u\bar{u}\bar{u}\to u\bar{u}\bar{u}} \mid^2$ is based on the same set of diagrams as $\mid \mathcal{M}_{\rm uu\bar{u}\to uu\bar{u}} \mid^2$, $\mid \mathcal{M}_{\rm u\bar{u}\bar{u}\to u\bar{u}\bar{u}} \mid^2$ is obtained from the expression of $\mid \mathcal{M}_{\rm uu\bar{u}\to uu\bar{u}} \mid^2$ by the replacements $s_{12} \to s_{23}$, $s_{23} \to s_{12}$, $s_{31} \to s_{31}$, $u_{12} \to u_{32}$, $u_{13} \to u_{31}$, $u_{21} \to u_{23}$, $u_{23} \to u_{21}$, $u_{31} \to u_{13}$ and $u_{32} \to u_{12}$. Similarly, $\mid \mathcal{M}_{\rm u\bar{u}\bar{d}\to u\bar{u}\bar{d}} \mid^2$ is obtained from $\mid \mathcal{M}_{\rm ud\bar{d}\to ud\bar{d}} \mid^2$, $\mid \mathcal{M}_{\rm ud\bar{u}\to ud\bar{u}} \mid^2$ from $\mid \mathcal{M}_{\rm udu\to udu} \mid^2$

and $\mid \mathcal{M}_{u\bar{d}\bar{d}\to u\bar{d}\bar{d}} \mid^2$ from $\mid \mathcal{M}_{uu\bar{d}\to uu\bar{d}} \mid^2$. These 3-to-3 quark-quark-antiquark scatterings bring more complexity to the evolution of quark matter than the 3-to-3 quark scatterings alone.

## 5. Numerical results from the particle sphere technique

The squared amplitudes $\mid \mathcal{M}_{uuu\to uuu} \mid^2$, $\mid \mathcal{M}_{uud\to uud} \mid^2$, $\mid \mathcal{M}_{udu\to udu} \mid^2$, $\mid \mathcal{M}_{udd\to udd} \mid^2$, $\mid \mathcal{M}_{uu\bar{u}\to uu\bar{u}} \mid^2$, $\mid \mathcal{M}_{uu\bar{d}\to uu\bar{d}} \mid^2$, $\mid \mathcal{M}_{ud\bar{u}\to ud\bar{u}} \mid^2$, $\mid \mathcal{M}_{ud\bar{d}\to ud\bar{d}} \mid^2$, $\mid \mathcal{M}_{u\bar{u}\bar{u}\to u\bar{u}\bar{u}} \mid^2$, $\mid \mathcal{M}_{u\bar{u}\bar{d}\to u\bar{u}\bar{d}} \mid^2$, $\mid \mathcal{M}_{u\bar{d}\bar{u}\to u\bar{d}\bar{u}} \mid^2$ and $\mid \mathcal{M}_{u\bar{d}\bar{d}\to u\bar{d}\bar{d}} \mid^2$ in Eq. (4) are calculated at $\alpha_{\rm s} = 0.5$ and the Coulomb exchange divergence that is encountered is removed by the use of a screening mass formulated in Refs. [22-24]. Gluon propagators in Feynman gauge are used in the squared amplitudes. A screening mass in these propagators leads to some gauge dependence. The transport equation is solved until momentum isotropy is established while up and down quarks and antiquarks each with number 250 are generated from the anisotropic parton momentum distribution (1) inside the volume of $-0.3$ fm $< z < 0.3$ fm and $r < 6.4$ fm.

When the interaction range is treated as being finite, a parton interacts only with surrounding partons. We define a sphere for a particle which is located at the center of the sphere. Every particle has a sphere and all the spheres have the same radius. The sphere is called particle sphere. The amount of particles in a sphere varies with the radius. The amount of particles also changes from one particle sphere to another. We denote the maximum amount of particles by $m_{\rm ps}$. The particle sphere radius is not the interaction range. When the sphere radius equals 1.6 fm, $m_{\rm ps} = 75$ is found for 1000 partons generated from the anisotropic parton momentum distribution. We only allow particles inside the sphere to scatter. But in the volume defined above this restriction still produces almost the same number of $n$-parton scatterings as that when no sphere is defined. Therefore, the restriction can produce accurate result in $n$-parton scatterings. Since the amount of particles inside a sphere is an order of magnitude lower than the total number of partons inside the volume, the operation of searching for scatterings is reduced considerably. For example, the total number of operations for searching 5-parton scatterings at time $t = 0.2$ fm/$c$ is $1000 m_{\rm ps}^4 \approx 3.2 \times 10^{10}$ with the use of particle spheres, which is dramatically smaller than the number $1000^5 = 10^{15}$ without the use of particle spheres. Particle spheres form a basic ingredient in our simulation of parton scatterings.

When a parton traverses inhomogeneous or evolved parton matter, the radius-fixed sphere of the parton contains different amounts of partons at different time. After a multi-parton scattering is finished, a particle sphere is determined for each final parton. Before or after a scattering event a parton possesses a different particle sphere. However, the particle sphere radius is always fixed at 1.6 fm independent of time. While parton matter expands, the amount of partons inside a particle sphere is reduced.

We define a scattering of two partons when the two partons have the closest distance less than the interaction range of $\sqrt{\sigma_{2\to 2}/\pi}$. The 2-to-2 scattering cross section $\sigma_{2\to 2}$ is calculated with the spin- and color-averaged squared amplitudes in Refs. [20,21] which are regulated by the screening mass $\mu_D$,

$$\sigma_{qq\to qq} = \sigma_{q\bar{q}\to q\bar{q}} = \frac{g_s^4}{16\pi s^2}\frac{8}{9}\left[s + 2\frac{s(s+2\mu_D^2)^2}{\mu_D^2(s+\mu_D^2)} + \frac{8}{3}(s+2\mu_D^2)\ln\frac{\mu_D^2}{s+\mu_D^2}\right] \qquad (5)$$

for the elastic scatterings of two quarks or antiquarks with the same flavor,

$$\sigma_{qq'\to qq'}=\sigma_{\bar{q}\bar{q}'\to\bar{q}\bar{q}'}=\sigma_{q\bar{q}'\to q\bar{q}'}=\frac{g_s^4}{16\pi s^2}\frac{4}{9}\left[s+\frac{2s(s+2\mu_D^2)^2}{\mu_D^2(s+\mu_D^2)}+2(s+2\mu_D^2)\ln\frac{\mu_D^2}{s+\mu_D^2}\right] \tag{6}$$

for the elastic scatterings of quarks and/or antiquarks with different flavors and

$$\sigma_{q\bar{q}\to q\bar{q}}=\frac{g_s^4}{16\pi s^2}\frac{8}{9}\left[\frac{s(s^2+3\mu_D^2 s+3\mu_D^4)}{3(s+2\mu_D^2)^2}+\frac{s(s+2\mu_D^2)^2}{\mu_D^2(s+\mu_D^2)}+\frac{2}{3}(s+2\mu_D^2)\ln\frac{\mu_D^2}{s+\mu_D^2}\right] \tag{7}$$

for the elastic scatterings of one quark and one antiquark with the same flavor.

Defining a 3-to-3 scattering event depends on the parton positions and flavors. If a three-parton scattering occurs, the three partons must be in a sphere of which the center is at the center-of-mass of the three partons and of which the radius $r_{hs}$ is [16]

$$\begin{aligned}\pi r_{hs}^2 &= \frac{1}{m}\int\frac{d^3p_4}{(2\pi)^3 2E_4}\frac{d^3p_5}{(2\pi)^3 2E_5}\frac{d^3p_6}{(2\pi)^3 2E_6}\\ &\quad\times(2\pi)^4\delta^4(p_1+p_2+p_3-p_4-p_5-p_6)\mid\mathcal{M}_{3\to3}\mid^2,\end{aligned} \tag{8}$$

where $m=1$ if $\mid\mathcal{M}_{3\to3}\mid^2=\mid\mathcal{M}_{ud\bar{u}\to ud\bar{u}}\mid^2$, $\mid\mathcal{M}_{ud\bar{d}\to ud\bar{d}}\mid^2$ or $\mid\mathcal{M}_{u\bar{u}\bar{d}\to u\bar{u}\bar{d}}\mid^2$, $m=2$ if $\mid\mathcal{M}_{3\to3}\mid^2=\mid\mathcal{M}_{uu\bar{u}\to uu\bar{u}}\mid^2$ or $\mid\mathcal{M}_{uu\bar{d}\to uu\bar{d}}\mid^2$, $m=4$ if $\mid\mathcal{M}_{3\to3}\mid^2=\mid\mathcal{M}_{u\bar{u}\bar{u}\to u\bar{u}\bar{u}}\mid^2$ or $\mid\mathcal{M}_{u\bar{d}\bar{d}\to u\bar{d}\bar{d}}\mid^2$. Since $\mid\mathcal{M}_{3\to3}\mid^2$ depends on the nine Lorentz-invariant momentum variables, we replace the phase-space integration by $du_{14}du_{24}du_{34}du_{15}du_{25}du_{35}$. However, this change is postponed to the next section.

The use of a finite interaction range in determining 2-to-2 and 3-to-3 scatterings breaks the locality of the transport equation and thus Lorentz covariance. But the particle subdivision technique [25,26] based on the transformation $f\to f'=\ell f$ can restore the Lorentz covariance. At $\ell=20$, a solution of Eq. (4) is taken as the average of 20 runs of Fortran code starting from different sets of partons generated from the distribution (1) at $t=0.2$ fm/$c$. The solution of the transport equation at the time of the order of 1.75 fm/$c$ is shown in Fig. 5 for various angles by the dotted, dashed and dot-dashed curves. The curves overlap and can thus be fitted to the Jüttner distribution,

$$f(\vec{p})=\frac{\lambda}{e^{|\vec{p}|/T}-\lambda}, \tag{9}$$

where the temperature of quark matter $T=0.27$ GeV and fugacity $\lambda=0.31$. We get a thermalization time of 1.55 fm/$c$.

## 6. Interaction range of three-parton scatterings

The radius of a sphere defined in Eq. (8) is Lorentz invariant and depends on $s_{12}$, $s_{23}$ and $s_{31}$. The integration over $\vec{p}_6$ gives

$$\pi r_{hs}^2=\frac{1}{m}\int\frac{d^3p_4}{(2\pi)^3 2E_4}\frac{d^3p_5}{(2\pi)^3 2E_5}\frac{2\pi}{2E_6}\delta(E_1+E_2+E_3-E_4-E_5-E_6)\mid\mathcal{M}_{3\to3}\mid^2. \tag{10}$$

Since $\mid\mathcal{M}_{3\to3}\mid^2$ is a function of the nine Lorentz-invariant momentum variables, we replace $d^3p_4$ and $d^3p_5$ with $du_{14}du_{24}du_{34}du_{15}du_{25}du_{35}$,

$$du_{14}du_{24}du_{34}=J_4 dp_{4x}dp_{4y}dp_{4z}, \tag{11}$$

$$du_{15}du_{25}du_{35} = J_5 dp_{5x}dp_{5y}dp_{5z}, \tag{12}$$

where $u_{14} = (p_1 - p_4)^2$, $u_{25} = (p_2 - p_5)^2$ and

$$J_4 = 8E_1E_2E_3 \mid (\vec{\mathrm{v}}_4 - \vec{\mathrm{v}}_1) \cdot [(\vec{\mathrm{v}}_4 - \vec{\mathrm{v}}_2) \times (\vec{\mathrm{v}}_4 - \vec{\mathrm{v}}_3)] \mid, \tag{13}$$

$$J_5 = 8E_1E_2E_3 \mid (\vec{\mathrm{v}}_5 - \vec{\mathrm{v}}_1) \cdot [(\vec{\mathrm{v}}_5 - \vec{\mathrm{v}}_2) \times (\vec{\mathrm{v}}_5 - \vec{\mathrm{v}}_3)] \mid, \tag{14}$$

where $\vec{\mathrm{v}}_\mathrm{i}$ is the velocity of the ith parton, and in the center-of-momentum frame the energies of three initial partons in the 3-to-3 scatterings are

$$E_1 = \frac{1}{2}\sqrt{\frac{(s_{31}^2 + s_s)(s_{12}^2 + s_s)}{s(s_{23}^2 + s_s)}}, \tag{15}$$

$$E_2 = \frac{1}{2}\sqrt{\frac{(s_{12}^2 + s_s)(s_{23}^2 + s_s)}{s(s_{31}^2 + s_s)}}, \tag{16}$$

$$E_3 = \frac{1}{2}\sqrt{\frac{(s_{23}^2 + s_s)(s_{31}^2 + s_s)}{s(s_{12}^2 + s_s)}}, \tag{17}$$

with $s_s = s_{12}s_{23} + s_{23}s_{31} + s_{31}s_{12}$ and the total energy of the three partons $E_1 + E_2 + E_3 = \sqrt{s} = \sqrt{s_{12} + s_{23} + s_{31}}$ is obtained from the definition $s = (p_1 + p_2 + p_3)^2$. Integrating over $u_{25}$ to remove $\delta(E_1 + E_2 + E_3 - E_4 - E_5 - E_6)$, so we get

$$\pi r_{\mathrm{hs}}^2 = -\frac{1}{m}\frac{1}{8(2\pi)^5}\int du_{14}du_{24}du_{34}du_{15}du_{35}\frac{\mid \mathcal{M}_{3\to 3} \mid^2}{E_4E_5E_6J_4J_5D}, \tag{18}$$

where in the center-of-momentum frame the energies of the three final partons are

$$E_4 = -\frac{u_{14} + u_{24} + u_{34}}{2\sqrt{s}}, \tag{19}$$

$$E_5 = -\frac{u_{15} + u_{25} + u_{35}}{2\sqrt{s}}, \tag{20}$$

$$\begin{aligned} E_6 \;=\; & \Bigg\{E_4^2 + E_5^2 - \frac{2}{d^2W_0}\Bigg[\left(W_{11}\frac{u_{15}}{2E_1} + W_{12}\frac{u_{25}}{2E_2} + W_{31}\frac{u_{35}}{2E_3}\right)\frac{u_{14}}{2E_1} \\ & + \left(W_{12}\frac{u_{15}}{2E_1} + W_{22}\frac{u_{25}}{2E_2} + W_{23}\frac{u_{35}}{2E_3}\right)\frac{u_{24}}{2E_2} \\ & + \left(W_{31}\frac{u_{15}}{2E_1} + W_{23}\frac{u_{25}}{2E_2} + W_{33}\frac{u_{35}}{2E_3}\right)\frac{u_{34}}{2E_3}\Bigg] + O_4O_5\Bigg\}^{\frac{1}{2}}, \end{aligned} \tag{21}$$

and the absolute value of the derivative of $E_1 + E_2 + E_3 - E_4 - E_5 - E_6$ with respect to $u_{25}$ is

$$\begin{aligned} D \;=\; & \Bigg|\frac{1}{2\sqrt{s}} - \frac{1}{2E_6}\Bigg[\frac{u_{15} + u_{25} + u_{35}}{2s} - \frac{1}{E_2d^2W_0}\left(W_{12}\frac{u_{14}}{2E_1} + W_{22}\frac{u_{24}}{2E_2} + W_{23}\frac{u_{34}}{2E_3}\right) \\ & + \frac{O_4}{2E_2O_5}\left(W_{220}\frac{u_{25}}{2E_2} + W_{120}\frac{u_{15}}{2E_1} + W_{230}\frac{u_{35}}{2E_3}\right)\Bigg]\Bigg|, \end{aligned} \tag{22}$$

which is evaluated at $u_{25}$ that is determined by the energy conservation relation $E_1+E_2+E_3-E_4-E_5-E_6=0$. Inside Eqs. (21) and (22),

$$d=(v_{1x}-v_{2x})(v_{1y}-v_{3y})-(v_{1y}-v_{2y})(v_{1x}-v_{3x}),$$

$$W_0=2(1-\vec{\mathrm{v}}_1\cdot\vec{\mathrm{v}}_2)(1-\vec{\mathrm{v}}_2\cdot\vec{\mathrm{v}}_3)(1-\vec{\mathrm{v}}_3\cdot\vec{\mathrm{v}}_1),$$

$$W_{\mathrm{i}}=v_{\mathrm{i}z}(\vec{\mathrm{v}}_{\mathrm{j}}-\vec{\mathrm{v}}_{\mathrm{k}})^2+v_{\mathrm{j}z}(\vec{\mathrm{v}}_{\mathrm{j}}-\vec{\mathrm{v}}_{\mathrm{k}})\cdot(\vec{\mathrm{v}}_{\mathrm{k}}-\vec{\mathrm{v}}_{\mathrm{i}})+v_{\mathrm{k}z}(\vec{\mathrm{v}}_{\mathrm{k}}-\vec{\mathrm{v}}_{\mathrm{j}})\cdot(\vec{\mathrm{v}}_{\mathrm{j}}-\vec{\mathrm{v}}_{\mathrm{i}}),$$

$$W_{\mathrm{ii}}=W_{\mathrm{i}}^2-W_0[(v_{\mathrm{j}x}-v_{\mathrm{k}x})^2+(v_{\mathrm{j}y}-v_{\mathrm{k}y})^2],$$

$$W_{\mathrm{ij}}=\frac{1}{2}(W_{\mathrm{kk}}-W_{\mathrm{ii}}-W_{\mathrm{jj}})$$

$$W_{\mathrm{ii0}}=W_{\mathrm{ii}}+W_0(v_{\mathrm{j}x}v_{\mathrm{k}y}-v_{\mathrm{j}y}v_{\mathrm{k}x})^2,$$

$$W_{\mathrm{ij0}}=W_{\mathrm{ij}}+W_0(v_{\mathrm{j}x}v_{\mathrm{k}y}-v_{\mathrm{j}y}v_{\mathrm{k}x})(v_{\mathrm{k}x}v_{\mathrm{i}y}-v_{\mathrm{k}y}v_{\mathrm{i}x}),$$

where the subscripts i, j and k allow the three cases: i = 1, j = 2, k = 3; i = 2, j = 3, k = 1; i = 3, j = 1, k = 2; and

$$\begin{aligned}O_{\mathrm{n}} \;=\; & \Bigg[W_{110}\left(\frac{u_{1\mathrm{n}}}{2E_1}\right)^2+W_{220}\left(\frac{u_{2\mathrm{n}}}{2E_2}\right)^2+W_{330}\left(\frac{u_{3\mathrm{n}}}{2E_3}\right)^2 \\ & +2W_{120}\frac{u_{1\mathrm{n}}}{2E_1}\frac{u_{2\mathrm{n}}}{2E_2}+2W_{230}\frac{u_{2\mathrm{n}}}{2E_2}\frac{u_{3\mathrm{n}}}{2E_3}+2W_{310}\frac{u_{1\mathrm{n}}}{2E_1}\frac{u_{3\mathrm{n}}}{2E_3}\Bigg]^{\frac{1}{2}},\end{aligned}$$

with n = 4, 5. The quantity $u_{25}$ determined by energy conservation gives

$$u_{26}=-s_{12}-s_{23}-u_{24}-u_{25} \tag{23}$$

that appears in $\mid \mathcal{M}_{3\to 3} \mid^2$. Replacing $u_{14}$ with $u_{16}$ in $u_{14}=-(s_{12}+s_{31}+u_{15}+u_{16})$, we obtain

$$\pi r_{\mathrm{hs}}^2=-\frac{1}{m}\frac{1}{8(2\pi)^5}\int du_{15}du_{16}du_{24}du_{34}du_{35}\frac{\mid \mathcal{M}_{3\to 3} \mid^2}{E_4E_5E_6J_4J_5D}. \tag{24}$$

The variables $u_{15}$, $u_{16}$, $u_{24}$, $u_{34}$ and $u_{35}$ have different minima:

$$u_{1\mathrm{min}}=-\sqrt{(s_{31}^2+s_s)(s_{12}^2+s_s)/(s_{23}^2+s_s)}=-(s_{31}+s_{12}), \tag{25}$$

for $u_{15}$ and $u_{16}$,

$$u_{2\mathrm{min}}=-\sqrt{(s_{12}^2+s_s)(s_{23}^2+s_s)/(s_{31}^2+s_s)}=-(s_{12}+s_{23}), \tag{26}$$

for $u_{24}$ and

$$u_{3\mathrm{min}}=-\sqrt{(s_{23}^2+s_s)(s_{31}^2+s_s)/(s_{12}^2+s_s)}=-(s_{23}+s_{31}), \tag{27}$$

for $u_{34}$ and $u_{35}$. In the center-of-momentum frame $E_4+E_5+E_6=\sqrt{s}$ and $\vec{p}_4+\vec{p}_5+\vec{p}_6=0$. While the three vectors $\vec{p}_4$, $\vec{p}_5$ and $\vec{p}_6$ are parallel, $\mid \vec{p}_4 \mid$, $\mid \vec{p}_5 \mid$ or $\mid \vec{p}_6 \mid$ takes its maximum $\sqrt{s}/2$. If, for example, $\vec{p}_1$ and $\vec{p}_5$ point to opposite directions and $\vec{p}_1$, $\vec{p}_4$ and $\vec{p}_6$ point to the same direction, $u_{15}$ by its definition reaches $-2E_1\sqrt{s}$, i.e. its minimum. Hence, when one of variables $u_{15}$, $u_{16}$, $u_{24}$, $u_{34}$ and $u_{35}$ takes its minimum, the three vectors $\vec{p}_4$,

$\vec{p}_5$ and $\vec{p}_6$ and one of $\vec{p}_1$, $\vec{p}_2$ and $\vec{p}_3$ are parallel. The minima set useful bounds to the Lorentz-invariant momentum variables by

$$u_{14} + u_{15} + u_{16} = u_{1\min} \tag{28}$$

$$u_{24} + u_{25} + u_{26} = u_{2\min} \tag{29}$$

$$u_{34} + u_{35} + u_{36} = u_{3\min} \tag{30}$$

with $u_{36} = (p_3 - p_6)^2$. Eq. (28) means that $u_{15}$ and $u_{16}$ cannot take the minimum $u_{1\min}$ at the same time. If $u_{15} = u_{1\min}$, $u_{14} = u_{16} = 0$. Eq. (28) is a plane equation in three-dimensional space. The distances of the $u_{14}$-intercept, $u_{15}$-intercept and $u_{16}$-intercept of the plane to the origin are the same, $-u_{1\min}$. Since $u_{14} < 0$, $u_{15} < 0$ and $u_{16} < 0$, the regions of the three variables are the interior of the triangle in the plane of which the three sides connect the $u_{14}$-intercept, $u_{15}$-intercept and $u_{16}$-intercept. The triangle is an equilateral triangle that has a side length of $-\sqrt{2}u_{1\min}$. Similar discussion applies to Eqs. (29) and (30). The three planes indicated by Eqs. (28)-(30) are parallel.

## 7. Summary

We have derived squared amplitudes for $qq\bar{q} \to qq\bar{q}$ and $q\bar{q}\bar{q} \to q\bar{q}\bar{q}$ at the tree level. Feynman diagrams depicted in Figs. 3 and 4 show the 3-to-3 scatterings which lead to the interplay of quark matter and antiquark matter. These squared amplitudes form new contributions in transport equations for quarks and antiquarks. We have presented the particle sphere technique to solve the transport equations while the formula for the interaction range of three partons is obtained by an integration over the Lorentz-invariant momentum variables in the equilateral triangle regions. It is shown by the solutions of the transport equations that the thermalization time of quark matter and antiquark matter is of the order of about 1.55 fm/$c$. This reduced thermalization time is an effect of quark-quark-antiquark and quark-antiquark-antiquark elastic scatterings that suggests the importance of multi-parton scatterings at high parton number density. Another interesting effect of three-body elastic scattering is shown on heavy quark momentum degradation in quark-gluon plasma [27].

## Acknowledgements

This work was supported in part by the National Natural Science Foundation of China under Grant No. 10675079. X.-M. thanks C.M. Ko for bringing his interesting work to the author's attention during quark matter 2006 conference at Shanghai.

## References


[1]STAR Collaboration, J. Adams, Nucl. Phys. **A757** (2005) 102.
[2]PHENIX Collaboration, K. Adcox, Nucl. Phys. **A757** (2005) 184.
[3]E. Shuryak, Phys. Rev. Lett. **68** (1992) 3270.
[4]K. Geiger, Phys. Rev. **D46** (1992) 4965;
K. Geiger, Phys. Rev. **D46** (1992) 4986.
[5]G.R. Shin, B. Müller, J. Phys. **G29** (2003) 2485.
[6]Z. Xu, C. Greiner, Phys. Rev. **C71** (2005) 064901.
[7]S.M.H. Wong, Phys. Rev. **C54** (1996) 2588.
G.C. Nayak, A. Dumitru, L. McLerran, W. Greiner, Nucl. Phys. **A687** (2001) 457.
[8]P.F. Kolb, P. Huovinen, U. Heinz, H. Heiselberg, Phys. Lett. **B500** (2001) 232.
P. Huovinen, Nucl. Phys. **A715** (2003) 299c.
[9]D. Teaney, J. Lauret, E.V. Shuryak, nucl-th/0110037.
E.V. Shuryak, Nucl. Phys. **A715** (2003) 289c.
[10]T. Hirano, Phys. Rev. **C65** (2001) 011901.
K. Morita, S. Muroya, C. Nonaka, T. Hirano, Phys. Rev. **C66** (2002) 054904.
[11]K.J. Eskola, H. Niemi, P.V. Ruuskanen, S.S. Räsänen, Phys. Lett. **B566** (2003) 187;
K.J. Eskola, H. Niemi, P.V. Ruuskanen, S.S. Räsänen, Nucl. Phys. **A715** (2003) 561c.
[12]X.-M. Xu, R. Peng, H.J. Weber, Phys. Lett. **B629** (2005) 68.
[13]K.J. Eskola, K. Kajantie, K. Tuominen, Phys. Lett. **B497** (2001) 39.
[14]M. Gyulassy, P. Lévai, I. Vitev, Nucl. Phys. **B594** (2001) 371;
M. Gyulassy, I. Vitev, X.-N. Wang, P. Huovinen, Phys. Lett. **B526** (2002) 301.
[15]F. Cooper, E. Mottola, G.C. Nayak, Phys. Lett. **B555** (2003) 181.
[16]X.-M. Xu, Y. Sun, A.-Q. Chen, L. Zheng, Nucl. Phys. **A744** (2004) 347.
[17]X.-N. Wang, M. Gyulassy, Phys. Rev. **D44** (1991) 3501;
M. Gyulassy, X.-N. Wang, Comput. Phys. Commun. **83** (1994) 307;
X.-N. Wang, Phys. Rep. **280** (1997) 287.
[18]P. Lévai, B. Müller, X.-N. Wang, Phys. Rev. **C51** (1995) 3326.
[19]R.D. Field, *Applications of Perturbative QCD*, Addison-Wesley, Redwood City, 1989.
[20]R. Cutler, D. Sivers, Phys. Rev. **D17** (1978) 196.
[21]B.L. Combridge, J. Kripfganz, J. Ranft, Phys. Lett. **B70** (1977) 234.
[22]T.S. Biró, B. Müller, X.-N. Wang, Phys. Lett. **B283** (1992) 171.
[23]K.J. Eskola, B. Müller, X.-N. Wang, Phys. Lett. **B374** (1996) 20.
[24]S.A. Bass, B. Müller, D.K. Srivastava, Phys. Lett. **B551** (2003) 277.
[25]B. Zhang, M. Gyulassy, Y. Pang, Phys. Rev. **C58** (1998) 1175.
[26]D. Molnár, M. Gyulassy, Nucl. Phys. **A697** (2002) 495.
[27]W. Liu, C.M. Ko, nucl-th/0603004.

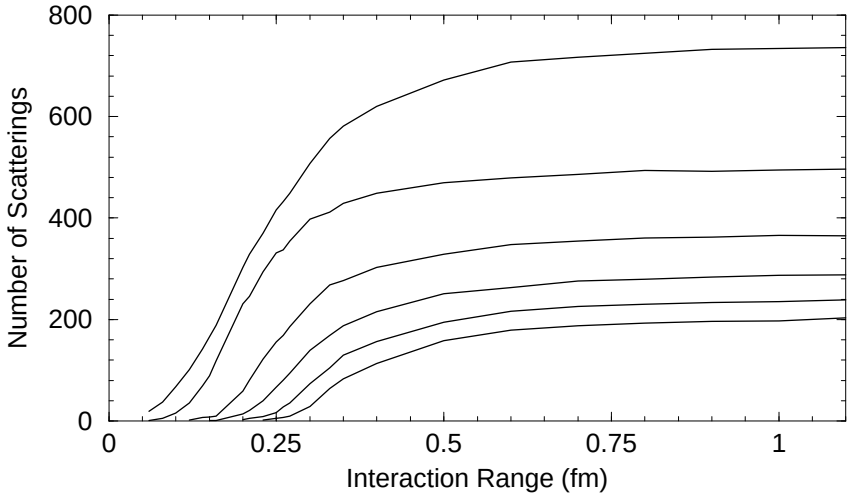


Figure 1: Curves from top to bottom show the numbers of $n$-parton scatterings with $n = 2, \cdots, 7$, respectively.

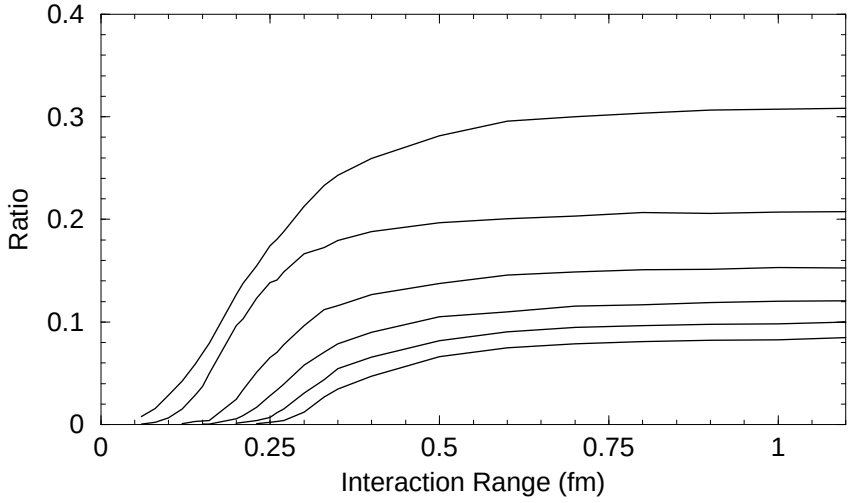


Figure 2: Curves from top to bottom show the ratio $R_n$ with $n = 2, \cdots, 7$, respectively.

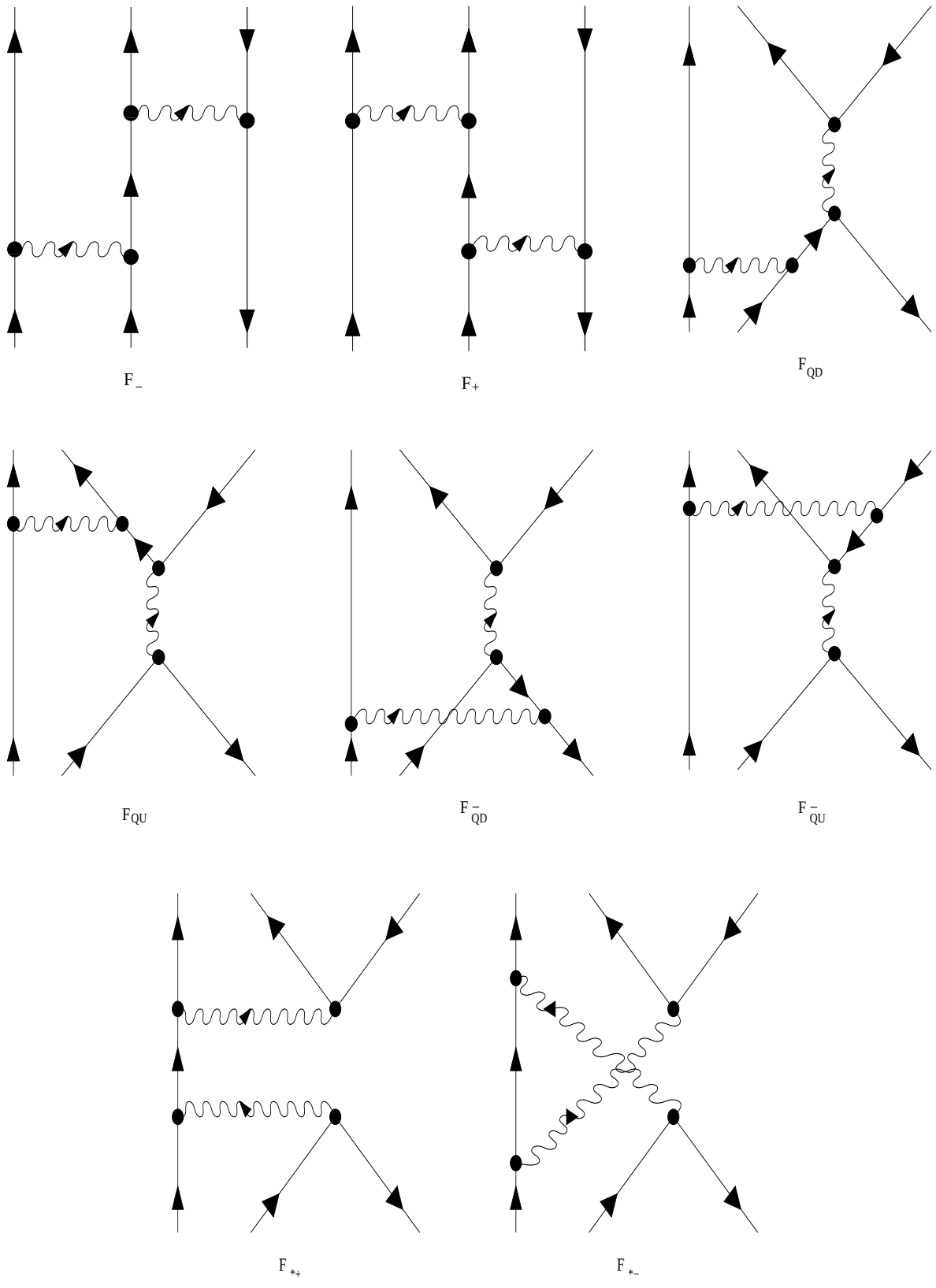


Figure 3: Two-gluon-exchange induced scatterings of two quarks and one antiquark.

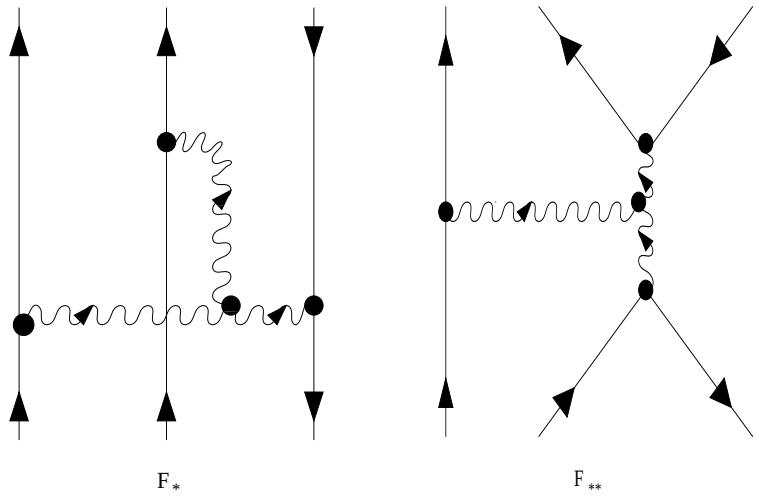


Figure 4: Triple-gluon coupling in quark-quark-antiquark scatterings.

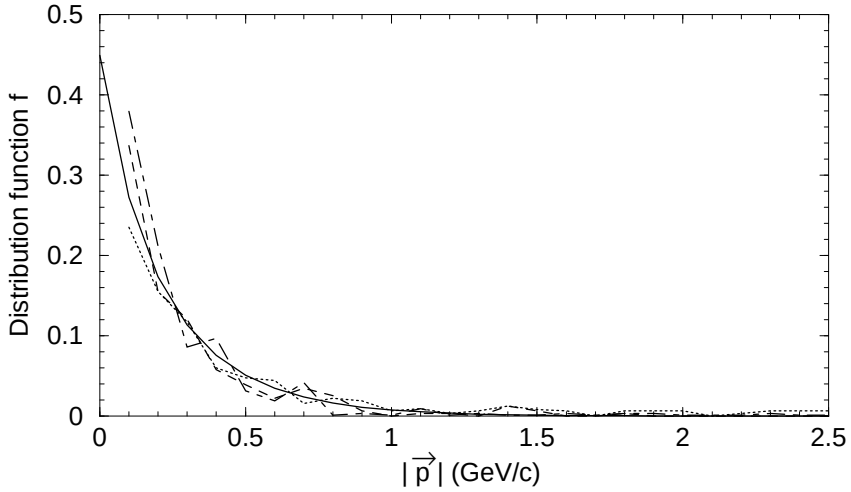


Figure 5: Quark distribution functions versus momentum in different directions while quark matter arrives at thermal equilibrium. The dotted, dashed and dot-dashed curves correspond to the angles relative to one incoming beam direction $\theta = 0^{\rm o}, 45^{\rm o}, 90^{\rm o}$, respectively. The solid curve represents the thermal distribution function.